ACS Sustainable Chemistry & Engineering

Subscriber access provided by The Bodleian Libraries of the University of Oxford

Article

Achieving highly selective electrocatalytic CO2 reduction by tuning CuO-Sb2O3 nanocomposites

Yangmei Li, Senlin Chu, Huidong Shen, Qineng Xia, Alex W. Robertson, Justus Masa, Umer Siddiqui, and Zhenyu Sun

ACS Sustainable Chem. Eng., **Just Accepted Manuscript** • DOI: 10.1021/acssuschemeng.0c00800 • Publication Date (Web): 02 Mar 2020

Downloaded from pubs.acs.org on March 13, 2020

Just Accepted

"Just Accepted" manuscripts have been peer-reviewed and accepted for publication. They are posted online prior to technical editing, formatting for publication and author proofing. The American Chemical Society provides "Just Accepted" as a service to the research community to expedite the dissemination of scientific material as soon as possible after acceptance. "Just Accepted" manuscripts appear in full in PDF format accompanied by an HTML abstract. "Just Accepted" manuscripts have been fully peer reviewed, but should not be considered the official version of record. They are citable by the Digital Object Identifier (DOI®). "Just Accepted" is an optional service offered to authors. Therefore, the "Just Accepted" Web site may not include all articles that will be published in the journal. After a manuscript is technically edited and formatted, it will be removed from the "Just Accepted" Web site and published as an ASAP article. Note that technical editing may introduce minor changes to the manuscript text and/or graphics which could affect content, and all legal disclaimers and ethical guidelines that apply to the journal pertain. ACS cannot be held responsible for errors or consequences arising from the use of information contained in these "Just Accepted" manuscripts.

is published by the American Chemical Society. 1155 Sixteenth Street N.W., Washington, DC 20036

Published by American Chemical Society. Copyright © American Chemical Society. However, no copyright claim is made to original U.S. Government works, or works produced by employees of any Commonwealth realm Crown government in the course of their duties.

Achieving highly selective electrocatalytic CO_2 reduction by tuning CuO-Sb_2O_3 nanocomposites

Yangmei Li,[a] Senlin Chu,[a] Huidong Shen,[a] Qineng Xia,*[b] Alex W. Robertson,*[c] Justus Masa,[d] Umer Siddiqui[a] and Zhenyu Sun*[a]

[a] State Key Laboratory of Organic–Inorganic Composites, College of Chemical Engineering, Beijing University of Chemical Technology, Beijing 100029, P. R. China

[b] College of Biological, Chemical Science and Engineering, Jiaxing University, Jiaxing 314001, Zhejiang, P. R. China

[c] Department of Materials, University of Oxford, Oxford, OX1 3PH, UK

[d] Analytische Chemie-Elektroanalytik & Sensorik, Ruhr-University Bochum, D-44780 Bochum, Germany

Corresponding author e-mail address: sunzy@mail.buct.edu.cn; xiaqineng@mail.zjxu.edu.cn; alex.w.robertson@gmail.com.

ABSTRACT: The development of highly active and selective electrocatalysts with low cost and earth abundance for electrochemical CO_2 reduction (ECR) remains an important area of interest. Here we report the modification of CuO with other metal (Bi, Sb, Cd and Zr) oxides to form bimetallic oxide nanocomposite catalysts exhibiting efficient ECR. In particular, CuO-Sb_2O_3 nanoparticles anchored on carbon black (CB) facilitated ECR selectively to CO at low overpotentials, providing a CO faradaic efficiency (FE) of up to 90.0% at –0.8 V versus reversible hydrogen electrode, in contrast to individual CuO/CB and Sb_2O_3/CB which gave rise to CO FEs of less than 31.0%, outperforming many previously reported catalysts. Strong interaction between CuO and Sb_2O_3 is found, which likely contributes to the enhanced ECR activity.

KEYWORDS: *CO_2 reduction, electrocatalysis, CO, CuO, Sb_2O_3*

INTRODUCTION

Renewable energy-powered electrochemical CO_2 reduction (ECR) to gaseous fuels or liquids with high energy densities offers a sustainable route for storing intermittent energy and managing the global carbon balance.[1-3] To achieve a high yield of targeted products, the design and discovery of new electrocatalysts is critical. Massive efforts have thus been made in the past decades to screen and develop a variety of electrocatalysts for CO_2 reduction.[4-10] CO, one of the reduction products of ECR, is an important feedstock that can be further converted into value-added chemicals via industrial Fisher-Tropsch process. Noble metals including Au,[11,12] Ag,[13,14] and Pd[15,16] have been demonstrated for ECR to produce CO with good catalytic activity. However, their high price and scarcity impede widespread practical application in ECR. Exploration of cost-effective and earth-abundant materials for efficient electrocatalytic CO_2 conversion is therefore highly demanded.

Creation of heterostructures with tunable components provides an effective way to enhance CO_2 adsorption and activation, thus facilitating ECR.[17-19] For example, alloying with

a second metal has been adopted to accelerate ECR by breaking the linear relationship between the binding strengths of different intermediates.[20] Various Cu alloys including Cu-Zn, Cu-Ni, Cu-Pb, Cu-Cd, Cu-Sn, and Cu-Ag have been investigated, which displayed catalytic behaviour distinct from single metals.[21] Alternatively, construction of metal/metal oxide hybrids has also been recognized to be beneficial to promoting CO_2 reduction performance.[22-24] A synergy between Au and CeO_x was demonstrated, which increased the stability of the carboxyl intermediate (*COOH), leading to much higher activity than Au or CeO_x alone for ECR. [23] The faradaic efficiency (FE) for CO formation over Au-CeO_x was 89.1% at an applied potential of –0.89 V versus reversible hydrogen electrode (*vs*. RHE). Despite these recent advances, interface engineering of multiple metal oxides for ECR has been rarely explored. We believe that properly tuning the composition and interaction of different metal oxides will allow one to improve reaction kinetics and optimize the binding of intermediates, and so achieve better electrocatalysis of CO_2 reduction.

In this work, we report the synthesis of CuO-Sb_2O_3 nanocomposites and demonstrate their application for enhanced ECR. CuO was selected for incorporation of a second phase because of its low cost, ready availability, tunable surface properties, and its renown to effectively catalyze ECR.[21] Importantly, the as-obtained CuO-Sb_2O_3 immobilized on carbon black (CB) was observed to greatly facilitate CO_2 reduction with a CO FE exceeding 80.0% in a wide potential range from –0.75 to –0.9 V (*vs*. RHE), reaching 90.0% at –0.8 V (*vs*. RHE), dramatically surpassing individual CuO and Sb_2O_3 with CO FEs of less than 31.0%. The product FE of CuO-Sb_2O_3/CB catalysts can be easily adjusted by taking advantage of the two metal oxide interactions with varying composition, interface contact, and microstructure. Moreover, possible enhancement in ECR activity is analyzed, which is closely associated with the strong interaction between the two metal oxides.

RESULTS AND DISCUSSION

Here the CuO-Sb_2O_3/CB catalysts were synthesized through a simple wet-chemical route with manipulation of composition, metal oxide loading, and structure (Table S1). Individual CuO/CB and Sb_2O_3/CB catalysts were also prepared as references for comparison. The X-ray diffraction (XRD) patterns of CuO/CB, Sb_2O_3/CB, and CuO-Sb_2O_3/CB (Cu-to-Sb mole ratio of 10:1) are provided in Fig. 1a. Two reflections at approximately 35.1 and 38.0° are clearly observed in CuO-Sb_2O_3/CB, which can be well assigned to the (002) and (111) planes of CuO, respectively. This indicates the yield of crystalline CuO in the CuO-Sb_2O_3/CB. We note that the two peaks shift to lower 2θ values compared to CuO/CB, possibly caused by the interactions of CuO and Sb_2O_3. Typical diffraction peaks corresponding to Sb_2O_3 are also identified in the CuO-Sb_2O_3/CB catalyst. The peak intensities are relatively lower than CuO due to the low percentage of Sb_2O_3 in the composite.

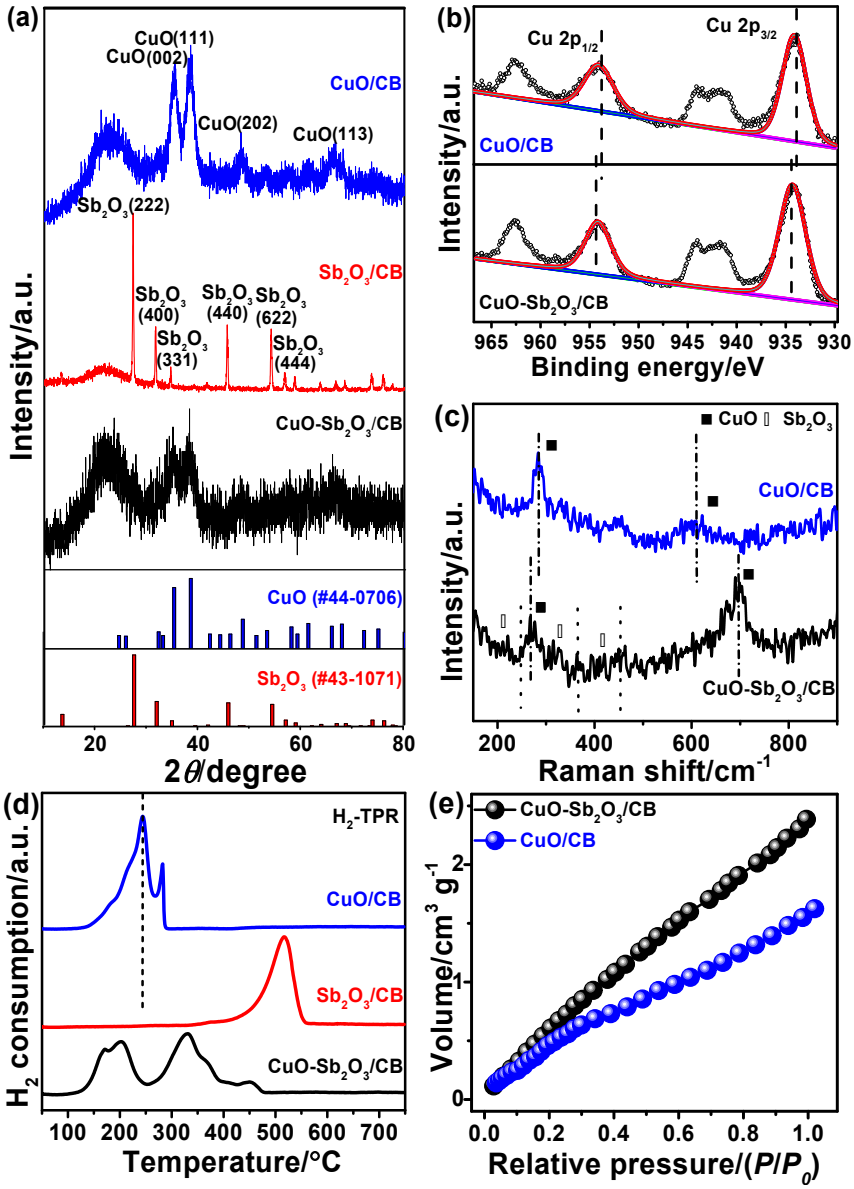


Figure 1. (a) XRD patterns of CuO/CB, Sb_2O_3/CB, and CuO-Sb_2O_3/CB. (b) Cu 2p XPS spectra and (c) Raman spectra of CuO/CB and CuO-Sb_2O_3/CB. (d) H_2-TPR diagrams of CuO/CB, Sb_2O_3/CB, and CuO-Sb_2O_3/CB. (e) CO_2 adsorption isotherms of CuO/CB and CuO-Sb_2O_3/CB. The molar ratio Cu and Sb in all the CuO-Sb_2O_3/CB is 10:1.

The chemical composition and electronic state of surface species in CuO-Sb_2O_3/CB samples were probed by X-ray photoelectron spectroscopy (XPS). The Cu 2p XPS spectrum of CuO/CB displays pronounced Cu $2p_{1/2}$ and $2p_{3/2}$ peaks with binding energies (BEs) at 953.8 and 933.9 eV,[12] respectively, along with their respective satellite peaks (Fig. 1b). An apparent shift of the Cu 2p BEs in CuO-Sb_2O_3/CB to higher values can be seen relative to the BEs of CuO/CB, implying electron transfer from Cu to Sb. Fig. S1 is the Sb 3d XPS spectrum of the CuO-Sb_2O_3/CB sample. It indicates Sb $3d_{3/2}$ and Sb $3d_{5/2}$ peaks at 539.8 and 530.4 eV respectively, which can be attributed to Sb (III).[24] These BEs are negatively shifted by ~0.2 eV compared to those of pure Sb_2O_3. The XPS results suggest alteration of the electronic

structures of CuO and Sb_2O_3, likely triggered by the lattice constant mismatch of the metal oxide interface.[28] The Raman spectrum of the CuO-Sb_2O_3/CB composite (Fig. 1c) reveals two apparent peaks at 283 and 621 cm^{-1} originating from CuO and three additional small peaks at 248, 374 and 448 cm^{-1} attributed to Sb_2O_3[26]. Notably, the characteristic peaks of CuO in the composite shift to higher wavenumbers compared to those observed for CuO/CB, which may indicate strong interaction between CuO and Sb_2O_3.

As illustrated in Fig. 1d, the temperature-programmed reduction of hydrogen (H_2-TPR) analysis showed two main peaks at about 200.0 and 325.0 °C, which correspond to the reduction of $Cu^{\delta+}$ to Cu^+ and Cu^+ to Cu^0 by consuming reducible oxygen from the CuO_x species in CuO-Sb_2O_3/CB. The first TPR peak shifts to lower temperature in the composite as compared to CuO/CB, likely due to spillover of H atoms (probably generated by the reduced Sb) to CuO. The second reduction peak occurs at a noticeably higher temperature which may result from the strong interaction of CuO and Sb_2O_3 and more difficulty in further reduction of Cu^+ to Cu^0. It is worth noting that CuO-Sb_2O_3/CB possesses significantly higher CO_2 adsorption capability than CuO/CB, as shown in Fig. 1e. This could result in enriched CO_2 on the local surface of the working electrode, being advantageous to CO_2 activation and reduction.

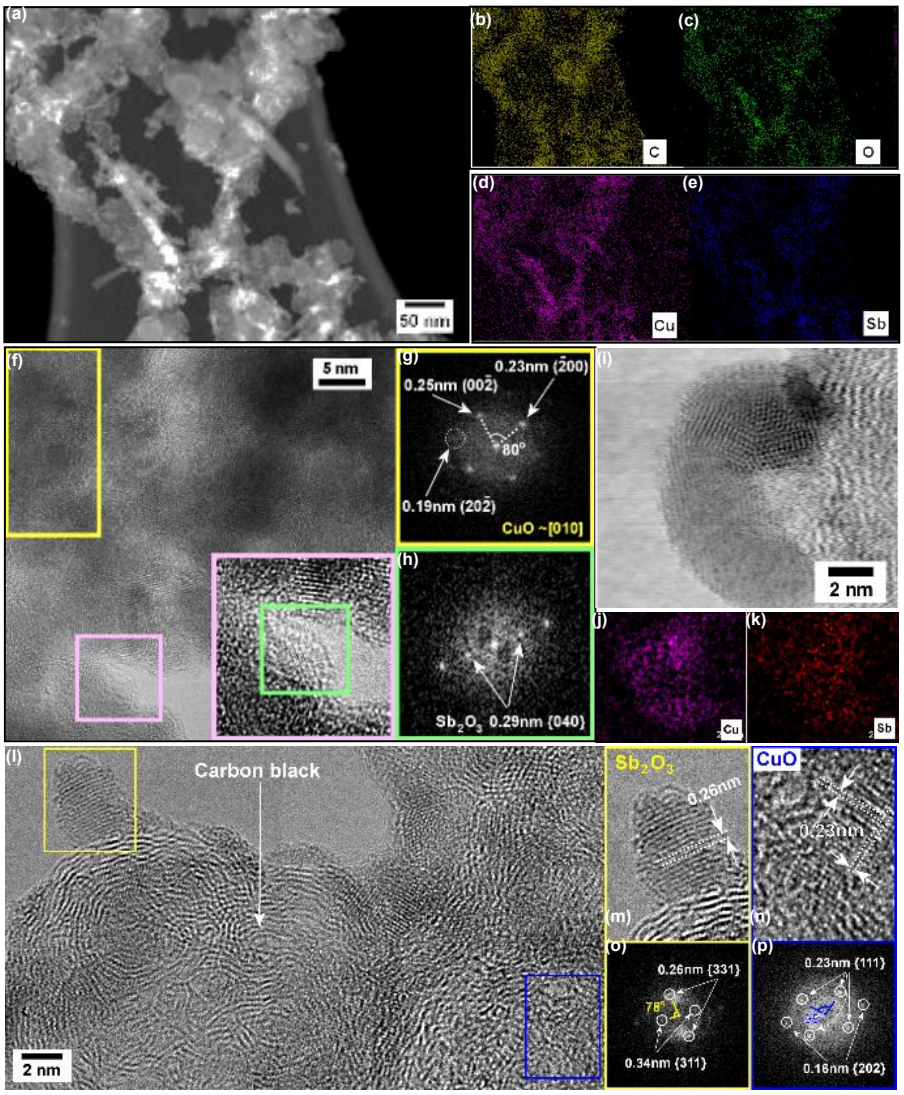


Figure 2. (a) HAADF-STEM image of CuO-Sb_2O_3/CB. EDS elemental maps of (b) C, (c) O, (d) Cu, and (e) Sb over the region shown in image a. (f) HRTEM image of CuO-Sb_2O_3/CB. The right bottom inset shows the magnified image of the region encased in the pink square. (g) and (h) correspond to Fast Fourier transforms (FFTs) of the areas encased in the yellow and green squares in image f, with g showing CuO viewed close to the [010] axis. (i) BF-STEM image of an individual CuO-Sb_2O_3 along with EDS elemental maps of Cu and Sb (j and k). (l) HRTEM image of CuO-Sb_2O_3/CB. (m-p) correspond to magnified image and corresponding FFTs of the regions encased by the yellow and blue rectangles in image l. The magnified CuO image in (n) was captured at a different defocus to (l), to aid visualizing the lattice structure. The molar ratio of Cu and Sb in all the cases is 10:1.

Transmission electron microscopy (TEM) equiped with energy-dispersive X-ray spectroscopy (EDS) was adopted to investigate the composition, morphology, and microstructure of the resulting CuO-Sb_2O_3/CB (Fig. 2). Aberration corrected high-angle annular dark-field scanning transmission electron microscopy (HAADF-STEM) combined with EDS maps (Fig. 2a-e) shows the presence of a number of CuO and Sb_2O_3 nanoparticles (NPs) that are uniformly distributed on CB. The average particle size is about 5 to 10 nm.

High-resolution TEM images (Fig. 2f and j), along with EDS maps and Fast Fourier transforms (FFTs) reveal the good crystallinity of the metal oxide NPs. Most Sb_2O_3 NPs were observed to have a large contact area with CuO NPs, as shown in Fig. 2f and i, with many particles overlapping into clusters, as displayed in Fig. 2f. A small fraction of Sb_2O_3 NPs are anchored on the surface of CB (Fig. 2l and m), which allowed us to image the structure of individual nanoparticles more clearly.

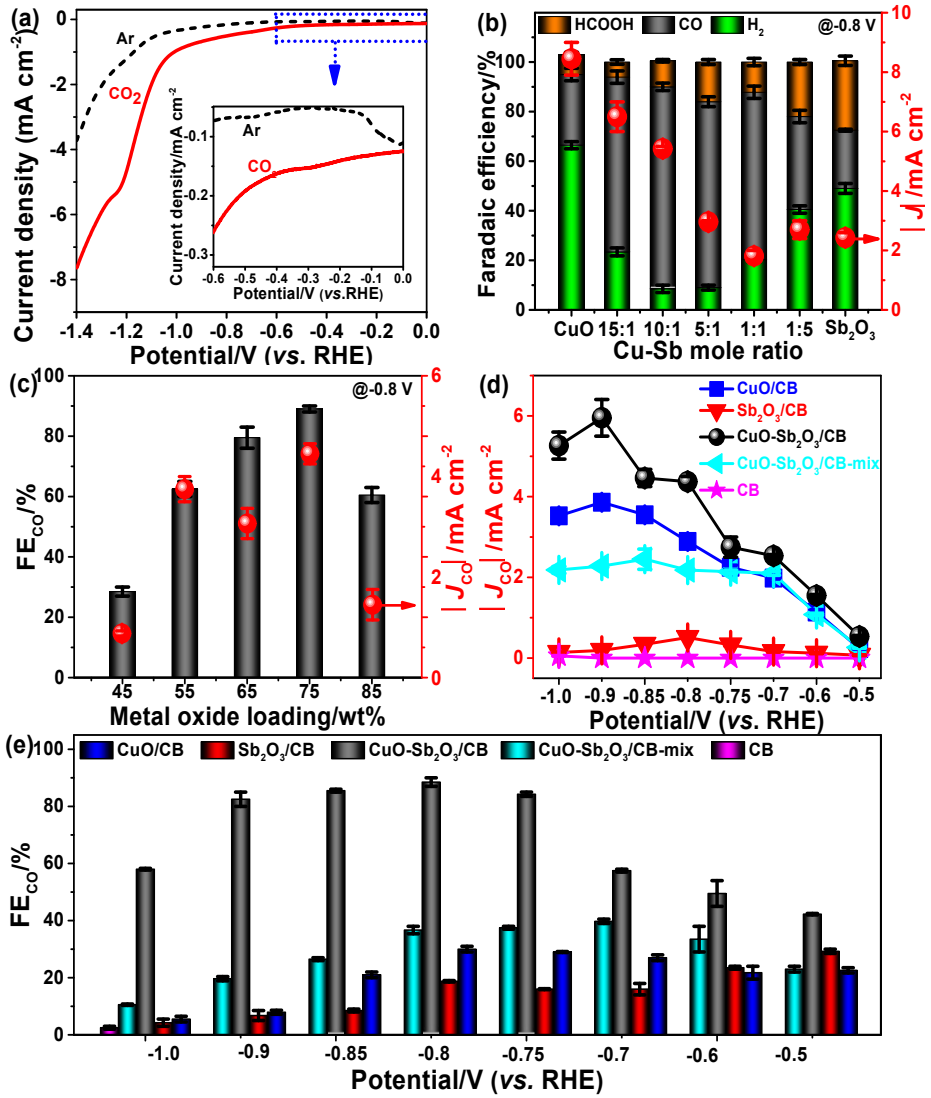


Figure 3. (a) LSV results of CuO-Sb_2O_3/CB on glassy carbon electrode in Ar-saturated (dashed black line) or CO_2-saturated (solid red line) 0.1 M aqueous $KHCO_3$ with a scan rate of 5.0 mV s^{-1}. (b) FE (bar) and current density (ball) of CuO-Sb_2O_3/CB as a function of Cu-to-Sb mole ratio for ECR in 0.1 M aqueous $KHCO_3$ at −0.8 V (*vs.* RHE). (c) CO FE and CO partial current density of CuO-Sb_2O_3/CB against metallic oxide loading at −0.8 V (*vs.* RHE). (d) CO partial current densities and (e) CO FEs of Sb_2O_3/CB, CuO/CB, CB, CuO-Sb_2O_3/CB, and CuO-Sb_2O_3/CB-mix at different applied potentials. The molar ratio of Cu and Sb in all CuO-Sb_2O_3/CB is 10:1 except in Fig. 3b. The metal oxide loading is 75.0 wt% in all the cases except in Fig. 3c. Standard errors were added in parts b, c, d, and e.

The CuO-Sb_2O_3/CB composite was evaluated as electrocatalysts for ECR in an H-type cell

(Fig. S2) separated by Nafion 117 at room temperature and atmospheric pressure.[27] All potentials here are relative to the RHE unless specified otherwise. Shown in Fig. 3a are the linear sweep voltammetry (LSV) plots of CuO-Sb_2O_3/CB in 0.1 M $KHCO_3$ solutions saturated with Ar and CO_2. It is apparent that the current densities of CuO-Sb_2O_3/CB in the CO_2-saturated electrolyte are substantially higher than that of Ar-saturated electrolyte, indicating predominant occurrence of CO_2 reduction. CO, H_2 and HCOOH were identified at applied potentials ranging from –0.4 to –1.0 V in a CO_2-saturated 0.1 M $KHCO_3$ solution (pH 6.8). CuO/CB exhibits rather low ECR activity with a CO FE of 31.0% and HCOOH FE of 1.1% at –0.8 V whereas Sb_2O_3/CB mainly reduces CO_2 to HCOOH with a FE of 30.0% (Fig. 3b). Interestingly, addition of a small amount of Sb_2O_3 in CuO remarkably inhibits the parasitic hydrogen evolution reaction (HER) and enhances ECR selectively to CO. The catalysts feature a composition-dependent product selectivity (Fig. 3b). The FE for CO formation increases with the increase of Sb_2O_3, reaching up to 90.0% at the Cu-to-Sb mole ratio of 10:1, whilst further increase of the Sb content leads to drop of the CO FE.

Keeping the Cu-to-Sb mole ratio constant at 10:1, we investigated the impact of bimetallic oxide loading content on CO_2 reduction. The CuO-Sb_2O_3 loading of 75.0 wt% was found to provide the best performance (Fig. 3c). To examine the possible synergistic effect of CuO/Sb_2O_3 interfaces on catalytic performance, we further compared CuO-Sb_2O_3/CB with pure CuO/CB, Sb_2O_3/CB, CB, and a physical mixture of CuO/CB and Sb_2O_3/CB (CuO-Sb_2O_3/CB-mix) for ECR at potentials from –1.0 to –0.5 V. The results show that the CuO-Sb_2O_3/CB composite catalyst outperforms all the other reference catalysts throughout the potential range (Fig. 3d and e), delivering CO FEs above 80.0% at potentials from –0.75 to –0.9 V. This indicates a synergy between CuO and Sb_2O_3 that facilitates CO_2-to-CO conversion. Note that the CuO-Sb_2O_3/CB is superior to CuO-Sb_2O_3/CB-mix for ECR, suggesting that an intimate contact to afford a large interface between the two metal oxides plays a role in enhancing electrocatalysis of CO_2 reduction to CO. The electrocatalytic properties were tunable and optimized by adjusting the quantity and feeding sequence of the metal salt precursors (Table S2).

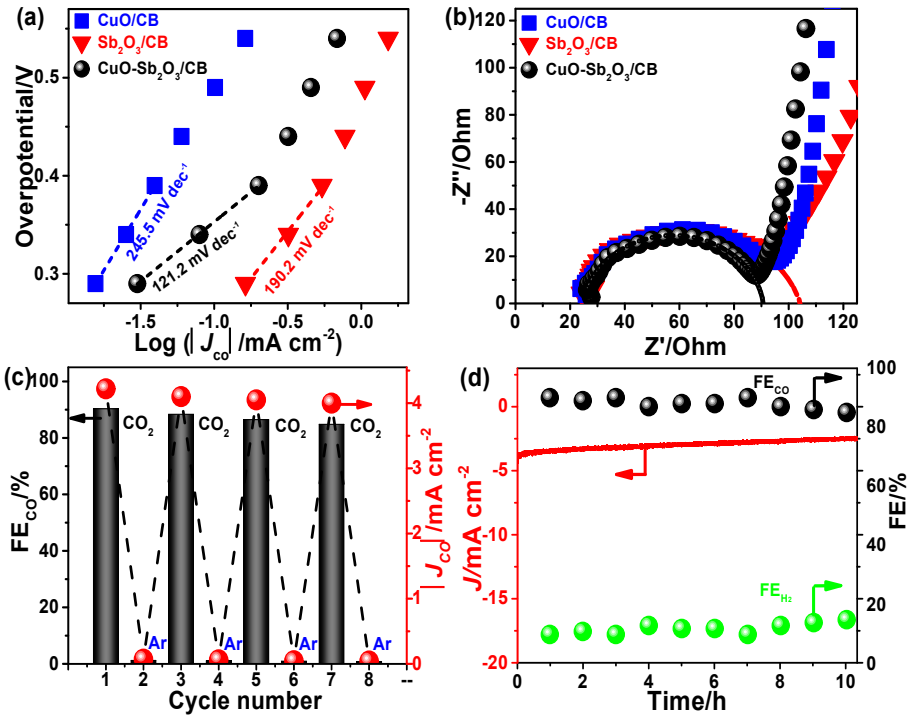


Figure 4. (a) Tafel plots and (b) EIS profiles of CuO-Sb_2O_3/CB, CuO/CB, and Sb_2O_3/CB. (c) CO FEs and CO partial current densities for CuO-Sb_2O_3/CB during cycles with an interval of 1 h in CO_2-saturated and Ar-saturated 0.1 M $KHCO_3$. (d) Current density, CO FE, and H_2 FE time responses of CuO-Sb_2O_3/CB at –0.8 V (*vs*. RHE).

The CO formation turnover frequency (TOF) was calculated and plotted aginst applied potential, as illustrated in Fig. S3. The CuO-Sb_2O_3/CB was found to exhibit a larger CO formation TOF than both individual CuO/CB and Sb_2O_3/CB. To further explain the remarkable activity of CuO-Sb_2O_3/CB, the electrochemical active surface area (ECSA), Tafel slope, and electrochemical impedance were probed. The as-made CuO-Sb_2O_3/CB exhibit larger double-layer capacitance than both CuO/CB and Sb_2O_3/CB (Fig. S4), indicative of its highest ECSA in the three catalysts, which is beneficial for ECR. Alternatively, CuO-Sb_2O_3/CB displays a Tafel slope of 121.2 mV dec^{-1}, less than 190.2 mV dec^{-1} for CuO/CB and 245.5 mV dec^{-1} for Sb_2O_3/CB (Fig. 4a), indicating that the former composite catalyst has faster kinetics for ECR than the latter two catalysts. This also implys that the first electron transfer to yield the *COOH intermediate on the catalyst surface determines the reaction rate for CO production.[10] Nyquist plots (Fig. 4b) show that the CuO-Sb_2O_3/CB catalyst facilitates more favorable interfacial charge transfer between the catalyst film and reactants in the electrolyte compared to CuO/CB and Sb_2O_3/CB, in agreement with its observed superior catalytic performance. Further,

Alternated electrolysis cycling measurements between Ar- and CO_2-saturated electrolytes show that the generated CO originates from the raw CO_2 and is stable even after eight cycles (Fig. 4c). In addition, the CuO-Sb_2O_3/CB catalyst retains reasonable stability without much

loss in CO FE and reduction current even after 10 h of successive electrolysis at –0.8 V (Fig. 4d). XPS measurements (Fig. S5) indicated increased surface percentages of Cu^0 and Sb^0 with prolonged electrolysis, resulting from reduction of the two metal oxides at the potential applied. It is inferred that surface Cu^0 and Sb^0 are probably the major catalytic active centers for CO_2 reduction.

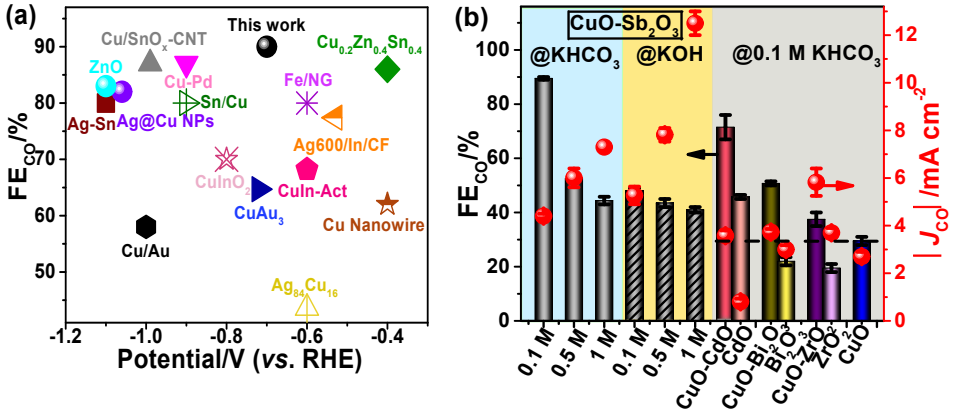


Figure 5. (a) Comparison of $CuO\text{-}Sb_2O_3$/CB with other reported electrocatalysts in terms of maximum CO FE. (b) CO partial current densities and CO FEs for $CuO\text{-}Sb_2O_3$/CB in various electrolytes with different concentrations and for many other CuO-based oxides as well as individual metal oxides.

It is worth noting that the performance of the $CuO\text{-}Sb_2O_3$/CB catalyst, in terms of maximum CO FE, exceeds many previously reported nanostructured Cu including Cu nanowires and Cu alloys such as CuAu, CuPd, CuSn, CuZnSn, and CuIn, and also other metal-based materials, as presented in Fig. 5a and Table S3. The impact of electrolyte on the performance of $CuO\text{-}Sb_2O_3$/CB for ECR was investigated in $KHCO_3$ and KOH solutions with different concentrations. Despite the decrease of CO FE with the increase of electrolyte concentration, the CO partial current density increases correspondingly, reaching 12.5 mA cm^{-2} at –0.8 V in 1.0 M KOH solution (Fig. 5b). The active sites of metal oxides and their mechanistic role and for CO_2 reduction are still a subject of ongoing discussion. The synergy between CuO and Sb_2O_3 for enhanced ECR may be explained from electronic and geometric effects. Enhanced electron density of Sb_2O_3, as indicated by XPS, facilitated the binding and stabilization of *COOH intermediate. From the geometric effect point of view, the surface of Sb_2O_3 is oxophilic, which also increased the affinity for *COOH. The stabilized *COOH species were adsorbed on an adjacent CuO center by interacting with one of the oxygen atoms, which were then converted to *CO at applied potentials and subsequently detached from the CuO surface.

Moreover, we also identified several other CuO-based metal oxides such as CuO-CdO, $CuO\text{-}Bi_2O_3$, and $CuO\text{-}ZrO_2$, which afford enhanced ECR compared with their respective individual components (Fig. 5b). Optimization of the ECR activity and exploration of cooperative effects in these catalytic systems are under way.

CONCLUSIONS

In summary, we have found a range of CuO-based bimetallic oxides that can effectively suppress hydrogen evolution and greatly promote electrocatalytic CO_2 reduction. Among the composite catalysts, the CuO-Sb_2O_3/CB enables efficient conversion of CO_2 to CO. The catalytic activity of CuO-Sb_2O_3/CB can be facilely regulated by changing the metal oxide loading and Cu-to-Sb mole ratio, leading to a CO FE as high as 90.0% at –0.8 V (*vs*. RHE) and a CO partial current density of 6.2 mA cm^{-2} at –0.9 V (*vs*. RHE), which makes it superior to many metal catalysts reported thus far. In addition, the CO FEs are more than 80.0% at applied potentials from –0.75 to –0.9 V (*vs*. RHE). The CO partial current density can be further improved to be 12.5 mA cm^{-2} in 1.0 M KOH electrolyte. Pronounced electron transfer occurs between Cu/Sb oxide interface, as confirmed by XPS, Raman, and H_2-TPR, which facilitates CO_2 adsorption and activation, thus enhancing ECR. Tuning of the interface structure by controlling exposed lattices of each metal oxide may further improve electrocatalysis of CO_2 reduction, which deserves future study.

ASSOCIATED CONTENT

Supporting Information

The Supporting Information is available free of charge on the ACS Publications website.

Experimental details; XPS spectra; C_{dl} and TOF plots of CuO/CB, Sb_2O_3/CB, and CuO-Sb_2O_3/CB; summary of some reported ECR catalysts

AUTHOR INFORMATION

Corresponding Authors

*(Z.S.) E-mail: sunzy@mail.buct.edu.cn.

*(Q.X.) E-mail: xiaqineng@mail.zjxu.edu.cn.

*(A.R.) E-mail: alex.w.robertson@gmail.com.

Author Contributions

Y.L. synthesized the samples and performed electrochemical tests. Y.L. and Z.S. wrote the paper. Z.S. supervised the project. All authors contributed to discussions on the work.

Notes

The authors declare no competing financial interest.

ACKNOWLEDGMENTS

This work was supported by the National Natural Science Foundation of China (No. 21972010, 21972056); Beijing Natural Science Foundation (No. 2192039); the State Key Laboratory of Organic–Inorganic Composites (No. oic-201901001); Beijing University of Chemical Technology (XK180301); UK EPSRC EP/K040375/1, for the South of England Analytical Electron Microscope. A.W.R. would like to thank the support of the Royal Society.

REFERENCES

(1) Sun, Z. Y.; Talreja, N.; Tao, H. C.; Texter, J.; Muhler, M.; Strunk, J.; Chen, J. F. Catalysis of carbon dioxide photoreduction on nanosheets: Fundamentals and challenges. *Angew. Chem. Int. Ed.* **2018**, *57*, 7610–7627, DOI org/10.1002/anie.201710509.

(2) Luna, P. D; Hahn, C.; Higgins, D.; Jaffer, S. A.; Jaramillo, T. F.; Sargent, E. H. What would it take for renewably powered electrosynthesis to displace petrochemical processes? *Science* **2019**, *364*, 3506, DOI 10.1126/science.aav3506.

(3) Gu, J.; Hsu, C. S.; Bai, L. C.; Chen, H. M.; Hu, X. L. Atomically dispersed Fe^{3+} sites catalyze efficient CO_2 electroreduction to CO. *Science* **2019**, *364*, 1091–1094, DOI 10.1126/science.aaw7515.

(4) Zheng, T. T.; Jiang, K.; Ta, N.; Hu, Y. F.; Zeng, J., Liu; J. Y.; Wang, H. T. large-scale and highly selective CO_2 electrocatalytic reduction on nickel single-atom catalyst. *Joule* **2019**, *3*, 265–278, DOI org/10.1016/j.joule. 2018. 10.015.

(5) Yang, H. P.; Wu, Y., Li; G. D., Lin; Q., Hu, Q.; Zhang, Q. L.; Liu, J. H.; He, C. X. Scalable production of efficient single-atom copper decorated carbon membranes for CO_2 electroreduction to methanol. *J. Am. Chem. Soc.* **2019**, *141*, 12717–12723, DOI org/10.1021/jacs.9b04907.

(6) Jia, M. W.; Fan, Q.; Liu, S. Z.; Qiu, J. S.; Sun, Z. Y. Single-atom catalysis for electrochemical CO_2 reduction. *Curr. Opin. Green Sustainable Chem.* **2019**, *16*, 1–6, DOI org/10.1016/j.cogsc.2018.11.002.

(7) Fan, Q.; Zhang, M. L.; Jia, M. W.; Liu, S. Z.; Qiu, J. S.; Sun, Z. Y. Electrochemical CO_2 reduction to C_{2+} species: Heterogeneous electrocatalysts, reaction pathways, and optimization strategies. *Mater. Today Energy* **2018**, *10*, 280–301, DOI org/10.1016/j.mtener.2018.10.003.

(8) Ma, T.; Fan, Q.; Tao, H. C.; Han, Z. S.; Jia, M. W.; Gao, Y. N.; Ma, W. J.; Sun, Z. Y. Heterogeneous electrochemical CO_2 reduction using nonmetallic carbon-based catalysts: Current status and future challenges. *Nanotechnology* **2017**, *28*, 472001, DOI org/10.1088/1361-6528/aa8f6f.

(9) Sun, Z. Y.; Ma, T.; Tao, H. C., Fan, Q.; Han, B. X. Fundamentals and challenges of electrochemical CO_2 reduction using two-dimensional materials. *Chem* **2017**, *3*, 560–587, DOI org/10.1016/j.chempr.2017.09.009.

(10) Jia, M. W.; Choi, C.; Wu, T. S.; Ma, C.; Kang, P.; Tao, H. C.; Fan, Q.; Hong, S.; Liu, S. Z.; Soo, Y. L.; Jung, Y. S.; Qiu, J. S.; Sun, Z. Y. Carbon-supported Ni nanoparticles for efficient CO_2 electroreduction. *Chem. Sci.* **2018**, *9*, 8775–8780, DOI 10.1039/C8SC03732A.

(11) Zhao, S.; Jin, R. X.; Jin, R. C. Opportunities and challenges in CO_2 reduction by gold- and silver-based electrocatalysts: From bulk metals to nanoparticles and atomically precise nanoclusters. *ACS Energy Lett.* **2018**, *3*, 452–462, DOI org/10.1021/acsenergylett.7b01104.

(12) Fu, J. J.; Zhu, W. L.; Chen, Y., Yin; Z. Y.; Li, Y. Y.; Liu, J.; Zhang, H. Y.; Zhu, J. J.; Sun, S. H. Bipyridine assisted assembly of Au nanoparticles on Cu nanowires to enhance electrochemical reduction of CO_2. *Angew. Chem. Int. Ed.* **2019**, *58*, 14100–14103, DOI org/10.1002/anie.201905318.

(13) Wang, R. M.; Haspel, H.; Pustovarenko, A.; Dikhtiarenko, A.; Russkikh, A.; Shterk, G.; Osadchii, D.; Chikh, S. O.; Ma, M.; Smith, W. A.; Takanabe, K.; Kapteijn, F.; Gascon, J. Maximizing Ag utilization in high-rate CO_2 electrochemical reduction with a coordination polymer-mediated gas diffusion electrode. *ACS Energy Lett.* **2019**, *4*, 2024–2031, DOI org/10.1021/acsenergylett.9b01509.

(14) Lu, Q.; Rosen, J.; Zhou, Y.; Hutchings, G. S.; Kimmel, Y. C.; Chen, J. G.; Jiao, F. A selective and efficient electrocatalyst for carbon dioxide reduction. *Nat. Commun.* **2014**, *5*, 3242, DOI: 10.1038/ncomms4242.

(15) Gao, D. F.; Zhou, H.; Cai, F.; Wang, J. G.; Wang, G. X.; Bao, X. H. Pd-containing nanostructures for electrochemical CO_2 reduction reaction. *ACS Catal.* **2018**, *8*, 1510–1519, DOI org/10.1021/acscatal.7b03612.

(16) Tao, H. C.; Sun, X. F.; Back, S.; Han, Z. S.; Zhu, Q. G.; Robertson, A. W.; Ma, T.; Fan, Q.; Han, B. X.; Jung,

Y. S.; Sun, Z. Y. Doping palladium with tellurium for highly selective electrocatalytic reduction of aqueous CO_2 to CO. *Chem. Sci.* **2018**, *9*, 483–487, DOI 10.1039/C7SC03018E.

(17) Choi, Y. W.; Scholten, F.; Sinev, I.; Cuenya, B. R. Enhanced stability and CO/formate selectivity of plasma-treated SnO_x/AgO_x catalysts during CO_2 electroreduction. *J. Am. Chem. Soc.* **2019**, *141*, 5261–5266, DOI org/10.1021/jacs.8b12766.

(18) Huo, S.; Weng, Z.; Wu, Z.; Zhong, Y.; Wu, Y.; Fang, J.; Wang, H. Coupled metal/oxide catalysts with tunable product selectivity for electrocatalytic CO_2 reduction. *ACS Appl. Mater. Interfaces* **2017**, *9*, 28519–28526, DOI org/10.1021/acsami.7b07707.

(19) Chu, S. L.; Hong, S.; Masa, J.; Li, X.; Sun, Z. Y. Synergistic catalysis of CuO/In_2O_3 composites for highly selective electrochemical CO_2 reduction to CO. *Chem. Commun.* **2019**, 55, 12380–12383, DOI org/10.1039/C9CC05435A.

(20) Vasileff, A.; Xu, C. C.; Jiao, Y.; Zheng, Y.; Qiao, S. Z. Surface and interface engineering in copper-based bimetallic materials for selective CO_2 electroreduction. *Chem,* **2018**, *4*, 1–23, DOI org/10.1016/j.chempr.2018.05.001.

(21) Watanabe, M.; Shibata, M.; Kato, A.; Azuma, M.; Sakata, T. Design of alloy electrocatalysts for CO_2 reduction III. The selective and reversible reduction of formula on Cu alloy electrodes. *J. Electrochem. Soc.* **1991**, *138*, 3382–3389, DOI org/site/terms_use.

(22) Larrazábal, G. O.; Martín, A. J.; Mitchell, S.; Hauert, R.; Ramírez, J. P. Synergistic effects in silver–indium electrocatalysts for carbon dioxide reduction. *J. Catal.* **2016**, *343*, 266–277, DOI org/10.1016/j.jcat.2015.12.014.

(23) Gao, D. F.; Zhang, Y.; Zhou, Z. W.; Cai, F., Zhao, X. F.; Huang, W. G.; Li, Y. S.; Zhu, J. F.; Liu, P.; Yang, F.; Wang, G. X.; Bao, X. H. Enhancing CO_2 electroreduction with the metal–oxide interface. *J. Am. Chem. Soc.* **2017**, *139*, 5652–5655, DOI org/10.1021/jacs.7b00102.

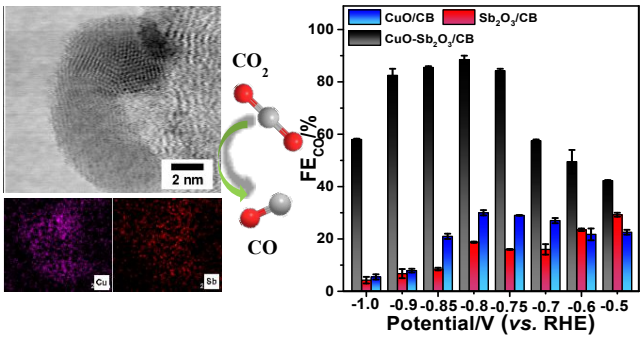
(24) Han, Z. S.; Choi, C.; Tao, H. C.; Fan, Q.; Gao, Y. N.; Liu, S. Z.; Robertson, W.; Hong, S.; Jung, Y.; Sun, Z. Y. Tuning Pd-catalyzed electroreduction of CO_2 to CO with reduced overpotential. *Catal. Sci. Techn.* **2018**, *8*, 3894–3900, DOI 10.1039/C8CY01037D.

(25) Zheng, Y.; Zhou, T.; Zhang, C.; Mao, J.; Liu, H.; Guo, Z. Boosted charge transfer in SnS/SnO_2 heterostructures: Toward high rate capability for sodium-ion batteries. *Angew. Chem. Int. Ed.* **2016,** 55, 3408–3413, DOI org/10.1002/anie.201510978.

(26) Zhao, Z. Q.; Hong, S.; Yan, C.; Choi, C.; Jung, Y.; Liu, Y. C.; Liu, S. Z.; Li, X., Qiu; J. S.; Sun; Z. Y. Efficient visible-light driven N_2 fixation over two-dimensional Sb/TiO_2 composites. *Chem. Commun.* **2019**, 55, 7171–7174, DOI org/10.1039/C9CC02291K.

(27) Fan, Q.; Choi, C.; Yan, C.; Liu, Y. C.; Qiu, J. S.; Hong, S.; Jung, Y.; Sun, Z. Y. High-yield production of few-layer boron nanosheets for efficient electrocatalytic N_2 reduction. *Chem. Commun.* **2019**, 55, 4246–4249, DOI org/10.1039/C9CC00985J.

Table of Contents



We report bimetallic CuO-Sb_2O_3 nanocomposites anchored on carbon black for selective electrocatalytic CO_2 reduction to CO.